J. Fluid Mech. (1998), *vol.* 361, *pp.* 25–39. Printed in the United Kingdom

Natural convection far downstream of a heat source on a solid wall

By F. J. HIGUERA[1] AND P. D. WEIDMAN[2]

[1]ETS Ingenieros Aeronáuticos, Plaza Cardenal Cisneros 3, 28040 Madrid, Spain

[2]Department of Mechanical Engineering, University of Colorado, Boulder, CO 80309 USA

(Received 8 August 1997 and in revised form 24 November 1997)

An analysis is presented of some steady natural convection flows at large distances downstream of point heat sources on solid walls. These asymptotic self-similar flows depend only on the Prandtl number of the fluid. The flow induced by a localized source on an adiabatic wall that is vertical or facing downwards is described numerically, whereas the flow due to a localized source on a wall facing upwards separates and leads to a self-similar plume. When the wall is held at the same temperature as the ambient fluid far from the source, the flow is described by a self-similar solution of the second kind, with the algebraic decay of the temperature excess above the ambient temperature determined by a nonlinear eigenvalue problem. Numerical solutions of this problem are presented for two-dimensional and localized heat sources on a vertical wall, whereas the problem for a localized heat source under an inclined isothermal downwards-facing wall turns out to capture the Rayleigh–Taylor instability of the flow and could not be solved by the methods used in this paper. The analogous flows in fluid-saturated porous media are found to be the solutions of parameter-free problems. A conservation law similar to the one holding for a wall jet is found in the case of a two-dimensional source on an isothermal wall and numerical solutions are presented for the other cases.

1. Introduction

Natural convection plumes originating from point or line sources of heat in an infinite expanse of otherwise quiescent fluid are of considerable interest in several engineering applications, including hot-wire anemometry, flows that arise in fires, and cooling of electronic circuitry. The asymptotic self-similar solutions describing these flows far downstream of their sources can be found in the early work of Zeldovich (1937), where it is pointed out that both flows very soon become unstable and then turbulent as the distance from the source increases, and the scalings for fully developed turbulent plumes are also worked out. The laminar plumes are more stable when the heat sources are embedded in adiabatic downward-facing solid walls, and the laminar two-dimensional wall plume arising from a line source of heat on a vertical or an inclined adiabatic wall has been extensively studied; see Zimin & Lyakhov (1970), Liburdy & Faeth (1975), Jaluria & Gebhart (1977), Sparrow, Patankar & Abdul-Wahed (1978), and Azfal (1980), among others. See also Gebhart *et al.* (1988) for a review.

The three-dimensional wall plumes arising from localized heat sources are of even greater practical importance than their two-dimensional analogues because real heat sources are of finite size. In particular, these flows are relevant to the cooling of electronic components in circuit boards. Carey & Mollendorf (1977) experimentally

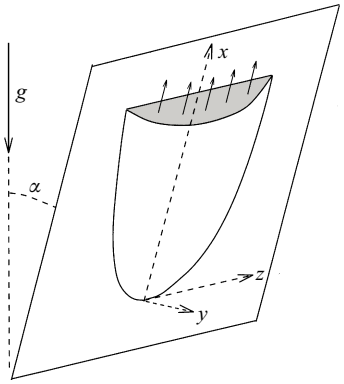

FIGURE 1. General schematic for the localized heat source problems.

investigated the water plume originating from a single square or circular thermofoil heater cemented on a vertical, approximately adiabatic Plexiglas sheet. These authors measured the temperatures of the fluid and of the wall above the heater using thermocouples and visualized the flow with schlieren photographs. From their experimental data, they concluded that the temperature excess decays proportionally to $x^{-0.77}$, the thickness of the plume, in the direction normal to the wall, increases linearly with x, and its width, in the spanwise direction, increases proportionally to $x^{1/5}$, where x is the vertical distance from the heater. Beyond this base configuration, the effects of interference between several heat sources, of additional bounding surfaces, and many other effects arising in practical applications to the cooling of electronic packages have been much studied, leading to a copious engineering literature (see Aung 1988; Kakac, Yüncü & Hijikata 1994; and Kim & Lee 1996).

In §2 of this paper the asymptotic self-similar structures of two natural convection flows are described. The first of these is the wall plume far downstream of a point source on an adiabatic non-horizontal wall and the second is the wall plume far downstream of a point or line source on a wall that is held at the same temperature as the ambient fluid far from the source. The scales of the flow, which are different for inclined and vertical walls, are easily worked out for the first of these problems, and the self-similar solutions are computed numerically. The second problem leads to self-similar solutions of the second kind, in which the rate of decay of the temperature with the distance from the source has to be determined as an eigenvalue of a nonlinear problem. Numerical solutions of this problem are presented for both line and point sources on vertical walls.

Self-similar planar and axisymmetric plumes in fluid-saturated porous media were studied by Wooding (1963), who showed that these problems are equivalent to those of planar and axisymmetric jets in Newtonian flow described by Bickley (1937) and Schlichting (1960); see also Nield & Bejan (1992). Wall plumes in porous media due to a point source on an adiabatic wall and to a point or line source on an isothermal wall are described in §3.

2. Newtonian flows

2.1. *Inclined, downward-facing adiabatic wall*

Consider the steady three-dimensional buoyant flow that evolves at very large distances downstream of a localized heat source on the surface of an insulated wall

facing downwards as sketched in figure 1. Assume that $0 < \alpha < \pi/2$. Let (x, y, z) be streamwise, plate-normal, and spanwise Cartesian coordinates, with (u, v, w) the corresponding velocity components, and $p = p_r/\rho_\infty$ where p_r is the excess reduced pressure above its value at infinity. Writing the fluid density in the form $\rho = \rho_\infty[1-\beta(T-T_\infty)]$ where T_∞ is the ambient temperature, the governing equations in the Boussinesq approximation, always applicable sufficiently far from the source, are

$$\nabla \cdot \boldsymbol{u} = 0, \tag{2.1}$$

$$\boldsymbol{u} \cdot \nabla u = -\frac{\partial p}{\partial x} + \theta \cos\alpha + \nu \nabla^2 u, \tag{2.2}$$

$$\boldsymbol{u} \cdot \nabla w = -\frac{\partial p}{\partial z} + \nu \nabla^2 w, \tag{2.3}$$

$$\boldsymbol{u} \cdot \nabla v = -\frac{\partial p}{\partial y} - \theta \sin\alpha + \nu \nabla^2 v, \tag{2.4}$$

$$\boldsymbol{u} \cdot \nabla \theta = \frac{\nu}{\sigma} \nabla^2 \theta, \tag{2.5}$$

wherein $\theta = g\beta(T - T_\infty)$. Far downstream of the heat source these equations are to be solved with the boundary conditions

$$y = 0: \quad \boldsymbol{u} = \boldsymbol{0}, \quad \frac{\partial \theta}{\partial y} = 0; \qquad (|z|, y) \to \infty: \quad \boldsymbol{u} = \boldsymbol{0}, \quad \theta = p = 0, \tag{2.6}$$

and the constraint that the heat flux passing any transverse section is constant, namely

$$\int_0^\infty \int_{-\infty}^\infty u\theta \, \mathrm{d}z \, \mathrm{d}y = \phi. \tag{2.7}$$

Here ν and β denote the kinematic viscosity and the coefficient of thermal expansion of the fluid; $\sigma = \nu/\kappa$, where κ is the thermal diffusivity, is the Prandtl number; and g is the acceleration due to gravity.

The scales of the variables $[z, y, u, w, \theta, p]$ in the asymptotic limit $x \to \infty$, identified with a subscript c in what follows, can be obtained from the following order of magnitude estimates: balancing streamwise advection, buoyancy, and plate-normal diffusion in (2.2) gives $u_c^2/x = \theta_c \cos\alpha = \nu u_c/y_c^2$; balancing advection and pressure gradient terms in (2.3) gives $u_c w_c/x = p_c/z_c$, where $u_c/x = w_c/z_c$ from (2.1); balancing the pressure gradient with buoyancy in (2.4) gives $p_c/y_c = \theta_c \sin\alpha$. Finally, the integral constraint (2.7) requires that $u_c\, \theta_c\, z_c\, y_c = \phi$ and closes the system. The solution of the six foregoing equations is given by

$$\left.\begin{aligned} z_c &= \frac{\nu^{1/3}(\tan\alpha)^{2/3}x^{7/9}}{Q^{1/9}}, \quad y_c = \frac{\nu^{2/3}(\tan\alpha)^{1/3}x^{5/9}}{Q^{2/9}}, \\ u_c &= \frac{Q^{4/9}}{\nu^{1/3}(\tan\alpha)^{2/3}x^{1/9}}, \quad w_c = \frac{Q^{1/3}}{x^{1/3}}, \\ \theta_c &= \frac{\phi}{Q^{1/9}\nu^{2/3}(\tan\alpha)^{1/3}x^{11/9}}, \quad p_c = \frac{Q^{2/3}}{x^{2/3}}, \end{aligned}\right\} \tag{2.8}$$

where $Q = \phi \sin\alpha$. These scales are based on viscous diffusion; alternative scales involving thermal diffusion, which are more appropriate at very small or very large Prandtl numbers, will be introduced later in this section. It is clear from (2.8) that $y_c/z_c \ll 1$ for $x \gg \nu^{3/2}/Q^{1/2}(\tan\alpha)^{3/2}$ and the boundary layer takes on a pancake-like structure as depicted in figure 1, for which the spanwise diffusion of momentum and heat are negligible. Also, advection and viscous forces are negligible in (2.4) which

reduces to a pressure–buoyancy equilibrium in the plate-normal direction; it is the spanwise gradient of this hydrostatic pressure distribution that pushes the fluid away from the symmetry plane. Plate-normal diffusion is of the same order as advection and pressure gradient in (2.3) and advection in (2.5). The x-dependence is now eliminated by the following transformation of variables:

$$\left.\begin{aligned} &z = z_c Z, \quad y = y_c Y, \\ &u = u_c\, U(Z,Y), \quad w = w_c\, W(Z,Y), \quad v = (u_c y_c/x)\, V(Z,Y), \\ &\theta = \theta_c\, \Theta(Z,Y), \quad p = p_c\, P(Z,Y). \end{aligned}\right\} \tag{2.9}$$

Substituting (2.9) into (2.1)–(2.7) gives the problem describing the leading-order structure of the cross-stream flow, which depends only on the Prandtl number. This problem can be rewritten in a somewhat simpler form by introducing the variables $\widetilde{W} = W - 7ZU/9$ and $\widetilde{V} = V - 5YU/9$, which are the scaled velocity components normal to the curvilinear coordinate surfaces $Z = \text{const.}$ and $Y = \text{const.}$; the problem now takes the form

$$\nabla_T \cdot \widetilde{\boldsymbol{V}} + \tfrac{11}{9}U = 0, \tag{2.10}$$

$$\widetilde{\boldsymbol{V}} \cdot \nabla_T U - \tfrac{1}{9}U^2 = \Theta + \frac{\partial^2 U}{\partial Y^2}, \tag{2.11}$$

$$\widetilde{\boldsymbol{V}} \cdot \nabla_T \widetilde{W} + \tfrac{4}{9}U\widetilde{W} - \tfrac{14}{81}ZU^2 = -\frac{\partial P}{\partial Z} - \tfrac{7}{9}Z\Theta + \frac{\partial^2 \widetilde{W}}{\partial Y^2}, \tag{2.12}$$

$$\frac{\partial P}{\partial Y} = -\Theta, \tag{2.13}$$

$$\widetilde{\boldsymbol{V}} \cdot \nabla_T \Theta - \tfrac{11}{9}U\Theta = \frac{1}{\sigma}\frac{\partial^2 \Theta}{\partial Y^2}, \tag{2.14}$$

$$Y = 0: \; U = \widetilde{W} = \widetilde{V} = \frac{\partial \Theta}{\partial Y} = 0; \quad (|Z|, Y) \to \infty: \; U = \widetilde{W} = \Theta = P = 0, \tag{2.15}$$

$$\int_0^\infty \int_{-\infty}^\infty U\Theta \, \mathrm{d}Z \, \mathrm{d}Y = 1. \tag{2.16}$$

Here, and in what follows, $\widetilde{\boldsymbol{V}} = (\widetilde{W}, \widetilde{V})$ and the gradient operator in the transverse plane ∇_T is defined as $(\partial/\partial Z,\ \partial/\partial Y)$.

A noteworthy feature of problem (2.10)–(2.16) is that it is not parabolic in Z, despite the absence of spanwise diffusion, because the pressure force driving the spanwise flow is not known in advance, but must be determined as part of the solution. In this respect the problem is similar to the natural convection flow induced by a downward-facing horizontal hot plate; see Higuera (1993). (See also Buckmaster 1973 and Lister 1992 for examples of this forcing mechanism in related problems.)

For the numerical treatment, problem (2.10)–(2.16) was discretized using finite differences and solved with a pseudo-transient method that essentially amounts to adding time derivatives to the left-hand sides of (2.11), (2.12) and (2.14) and marching in time until a steady solution is attained.

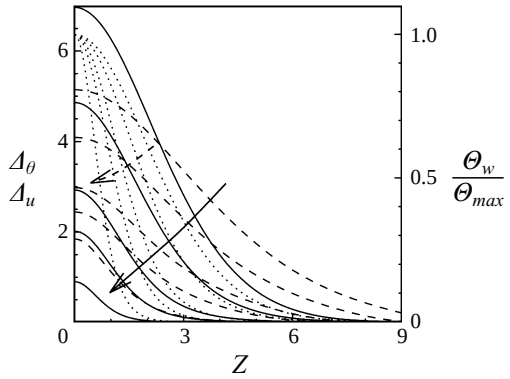

FIGURE 2. Thermal and viscous boundary layer thicknesses (solid and dashed, respectively, left-side scale) and wall temperature scaled with Θ_{max} (dotted, right-side scale) as functions of spanwise distance for $\sigma = 0.1$, 0.2, 0.5, 1, 5, and 10, increasing as indicated by the arrows.

The local thicknesses of the thermal and viscous boundary layers, defined as

$$\left.\begin{aligned} \Delta_\theta(Z) &= \frac{1}{\Theta_{max}} \int_0^\infty \Theta(Z,Y)\,\mathrm{d}Y, \\ \Delta_u(Z) &= \frac{1}{U_{max}} \int_0^\infty U(Z,Y)\,\mathrm{d}Y, \end{aligned}\right\} \tag{2.17}$$

where $\Theta_{max} = \Theta(0,0)$ and $U_{max} = \max_{Z,Y} U$ are the overall maximum temperature and velocity, are plotted in figure 2 for different values of σ. Also plotted in this figure is the wall temperature of each section, $\Theta_w = \Theta(Z,0)$, divided by Θ_{max}. As was to be expected, the thicknesses are maximum at the centreplane and decrease with spanwise distance. Both the thicknesses and the spanwise widths of the layer increase with decreasing σ, reflecting the increasing importance of thermal diffusion relative to viscous diffusion, the latter of which was used in the definition of the scaling factors (2.8). The thermal layer is thicker than the viscous layer for small values of σ and vice versa for large σ. Figure 2 also shows that the spanwise width of the viscous layer is larger than that of the thermal layer for any σ. This may be an effect of the slow decay with Z of $\Theta + U^2/9$, which acts as a forcing term in the momentum equation (2.11), compared with the faster decay of $11\,U\Theta/9$ in (2.14).

Other numerical results are given in figure 3 as functions of the Prandtl number σ. Plotted in this figure are $\Theta(0,0)$, which is the maximum value of $\Theta(Z,Y)$ and thus characterizes the decrease of temperature with x: $\theta \sim \Theta(0,0)\phi/\{Q^{1/9}\nu^{2/3}(\tan\alpha)^{1/3}x^{11/9}\}$; $\partial U/\partial Y$ at $(0,0)$, which similarly characterizes the shear stress on the wall; $\int_0^\infty \int_{-\infty}^\infty U\,\mathrm{d}Z\,\mathrm{d}Y$, the mass flux carried by the wall plume scaled with $Q^{1/9}\nu^{2/3}(\tan\alpha)^{1/3}x^{11/9}$ or, equivalently, the entrainment rate scaled with $\frac{11}{9}Q^{1/9}\nu^{2/3}(\tan\alpha)^{1/3}x^{2/9}$; and $\int_0^\infty \int_{-\infty}^\infty U^2\,\mathrm{d}Z\,\mathrm{d}Y$, the momentum flux scaled with $Q^{5/9}\nu^{1/3}x^{10/9}/(\tan\alpha)^{1/3}$, which is of interest for the evolution of the free plume that would develop beyond the upper edge of a large but finite wall.

The trends of the quantities displayed in figure 3 can be explained by reference to the asymptotic limits $\sigma \to 0$ and $\sigma \to \infty$, which are also of interest in themselves. In the limit $\sigma \to 0$ heat conduction reaches farther than viscous diffusion and the flow becomes effectively inviscid in the wall plume, with the exception of a relatively thin viscous sublayer by the wall which is required to enforce the no-

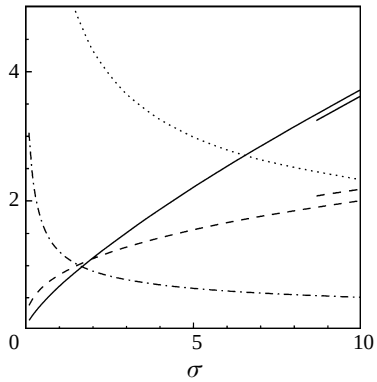

FIGURE 3. Values of $\Theta(0,0)$ (solid), $\partial U/\partial Y(0,0)$ (dashed), $\int U\,\mathrm{d}Z\,\mathrm{d}Y$ (dotted), and $\int U^2\,\mathrm{d}Z\,\mathrm{d}Y$ (dash-and-dot), as functions of the Prandtl number, from the numerical solution of (2.10)–(2.16). The short curves on the right-hand side are asymptotic results for $\sigma \to \infty$.

slip condition. Appropriate scales for the variables $(Z, Y, U, \widetilde{W}, \widetilde{V}, \Theta, P)$ outside the viscous sublayer are $(\sigma^{-1/3}, \sigma^{-2/3}, \sigma^{1/3}, 1, \sigma^{-1/3}, \sigma^{2/3}, 1)$, respectively, resulting from the balances of advection and buoyancy in (2.11), advection and pressure force in (2.12), and advection and conduction in (2.14). By rewriting (2.10)–(2.16) in rescaled variables, the factor σ disappears from (2.14) and reappears multiplying the viscous terms of (2.11) and (2.12). These viscous terms disappear in the limit $\sigma \to 0$ and the resulting inviscid problem is to be solved with the conditions $\widetilde{V} = \partial\Theta/\partial Y = 0$ at $Y = 0$, in place of the no-slip conditions in (2.15). From the numerical solution of this problem,

$$\left.\begin{aligned} &\Theta(0,0) \approx 0.611\,\sigma^{2/3} \\ &\int_0^\infty \int_{-\infty}^\infty U\,\mathrm{d}Z\,\mathrm{d}Y \approx \frac{6.22}{\sigma^{2/3}} \\ &\int_0^\infty \int_{-\infty}^\infty U^2\,\mathrm{d}Z\,\mathrm{d}Y \approx \frac{2.23}{\sigma^{1/3}} \end{aligned}\right\} \quad \text{for} \quad \sigma \to 0, \tag{2.18}$$

whereas $\partial U/\partial Y(0,0) = O(\sigma^{1/2})$ (using the estimate $Y = O(\sigma^{-1/6})$ in the relatively thin viscous sublayer).

In the opposite limit, $\sigma \to \infty$, the thermal layer is very thin and the effect of the inertia of the fluid is negligible in its interior, being important only in a thicker isothermal layer driven by the non-zero velocity extant at the outer edge of the thermal layer. Appropriate scales for the variables in the thermal layer, obtained from the balances of viscous diffusion and buoyancy or pressure forces in (2.11) and (2.12), and of advection and conduction in (2.14), are $(\sigma^{-2/9}, \sigma^{-4/9}, \sigma^{-1/9}, \sigma^{-1/3}, \sigma^{-5/9}, \sigma^{7/9}, \sigma^{1/3})$, written in the same order as before. The resulting limiting problem is given by (2.10)–(2.16) with the left-hand sides of (2.11) and (2.12) suppressed and the boundary conditions for $(|Z|, Y) \to \infty$ changed to $\partial U/\partial Y = \partial\widetilde{W}/\partial Y = \Theta = P = 0$. From the numerical solution of this problem,

$$\Theta(0,0) \approx 0.603\,\sigma^{7/9} \quad \text{and} \quad \frac{\partial U}{\partial Y}(0,0) \approx 1.015\,\sigma^{1/3} \quad \text{for} \quad \sigma \to \infty, \tag{2.19}$$

whereas $\int_0^\infty \int_{-\infty}^\infty U\,\mathrm{d}Z\,\mathrm{d}Y = O(\sigma^{-5/18})$ and $\int_0^\infty \int_{-\infty}^\infty U^2\,\mathrm{d}Z\,\mathrm{d}Y = O(\sigma^{-7/18})$ (using the estimate $Y = O(\sigma^{1/18})$ in the thick isothermal viscous layer). The asymptotic

results (2.19) have been included in figure 3, showing good agreement with the numerical solutions for σ large. The agreement of the numerical solutions for σ small with the results (2.18) is also good. These latter results have not been displayed in order not to clutter figure 3.

The stability of the solutions of (2.10)–(2.16) will not be analysed here. It may be worth noticing, however, that the velocity profiles of the present flow, whose Grashof number is proportional to $x^{8/9}$, are not unlike the profiles of two-dimensional natural convection boundary layers on vertical walls heated at a uniform temperature or supplying a uniform heat flux to the fluid, whose stability has been analysed by Nachtsheim (1963), Dring & Gebhart (1968), Haaland & Sparrow (1973*b*), and others. Therefore the stability characteristics of the two flows should be expected to be similar. Moreover, the maximum temperature is attained at the wall in the present solutions, so that the stratification is everywhere stable and the flow is free from the vortex instability mechanism that afflicts two-dimensional boundary layers on upward-facing inclined walls (Sparrow & Husar 1969; Lloyd & Sparrow 1970; Chen & Tzuoo 1982).

The case of a downward-facing horizontal wall ($\alpha = \pi/2$) differs from the one treated here in that the flow is driven only by the horizontal gradient of the hydrostatic pressure distribution generated by buoyancy in the warm fluid. Daniels (1992) showed that the problem of natural convection due to a line source of heat under an infinite adiabatic horizontal wall has no steady solution far away from the source, at least not of the self-similar type suggested by an order of magnitude analysis. This is because the buoyancy-induced pressure force would point toward the source in such a solution. The analogous problem for a point source, which would lead to a radial flow with a pressure force pointing inwards toward the source in the outer part of the boundary layer and outward in the vicinity of the wall, does not have a solution either.

No solution of the type considered in this section exists with a wall facing upwards ($\alpha < 0$) because then the buoyancy force is directed away from the wall and the spanwise pressure force is toward the symmetry plane, pinching the fluid from the sides and leading to the separation of the warm layer and the formation of a self-similar plume, the similarity properties of which are known (Zeldovich 1937).

2.2. *Vertical adiabatic wall*

The vertical plate represents a special limit that must be considered separately. This corresponds to the situation where a vertical plume is cut down its centreline by an infinitely thin insulated wall, and a scaling similar to that for a free unbounded plume may be expected. Indeed, diffusion occurs equally in both the spanwise and plate-normal directions ($z_c = y_c$) and the balances between advection, buoyancy, and viscous forces in the streamwise momentum equation, and between advection and pressure forces in the transverse momentum equations, along with the equation of continuity and the energy conservation condition (2.7), give the same scaling as for a vertical plume emanating from a point source in an unbounded fluid, as first reported by Zeldovich (1937), namely

$$\left.\begin{aligned} u_c &= \left(\frac{\phi}{\nu}\right)^{1/2}, \quad \theta_c = \frac{\phi}{\nu x}, \quad p_c = \frac{(\phi\nu)^{1/2}}{x}, \\ z_c &= y_c = \frac{\nu^{3/4}x^{1/2}}{\phi^{1/4}}, \quad w_c = v_c = \frac{(\phi\nu)^{1/4}}{x^{1/2}}. \end{aligned}\right\} \tag{2.20}$$

Transforming dependent and independent variables according to (2.9) with the scales given in (2.20) and introducing the new tilde variables $\widetilde{W} = W - ZU/2$ and $\widetilde{V} = V - YU/2$ yields the equations governing the transverse structure of the wall plume:

$$\nabla_T \cdot \widetilde{\boldsymbol{V}} + U = 0, \tag{2.21}$$

$$\widetilde{\boldsymbol{V}} \cdot \nabla_T U = \Theta + \nabla_T^2 U, \tag{2.22}$$

$$\widetilde{\boldsymbol{V}} \cdot \nabla_T \widetilde{\boldsymbol{V}} - \tfrac{1}{4} U^2 \boldsymbol{X} = -\nabla_T P - \tfrac{1}{2} \Theta \boldsymbol{X} + \nabla_T^2 \widetilde{\boldsymbol{V}} + \nabla_T U, \tag{2.23}$$

$$\widetilde{\boldsymbol{V}} \cdot \nabla_T \Theta - U\Theta = \frac{1}{\sigma} \nabla_T^2 \Theta, \tag{2.24}$$

to be solved with the boundary conditions

$$\left.\begin{aligned} Y = 0 :\ & U = \widetilde{W} = \widetilde{V} = \frac{\partial \Theta}{\partial Y} = 0, \\ (|Z|, Y) \to \infty :\ & U = \widetilde{W} = \widetilde{V} = \Theta = P = 0, \end{aligned}\right\} \tag{2.25}$$

and integral constraint (2.16). Again $\widetilde{\boldsymbol{V}} = (\widetilde{W}, \widetilde{V})$ and here and in what follows $\boldsymbol{X} = (Z, Y)$.

For the numerical treatment, the transverse velocity components were written in the form $\widetilde{W} = \partial \widetilde{\Phi}/\partial Z + \partial \widetilde{\Psi}/\partial Y$ and $\widetilde{V} = \partial \widetilde{\Phi}/\partial Y - \partial \widetilde{\Psi}/\partial Z$, where $\nabla_T^2 \widetilde{\Phi} = -U$ from (2.21) and $\nabla_T^2 \widetilde{\Psi} = -\widetilde{\Omega}$. Here $\widetilde{\Omega} \equiv \partial \widetilde{V}/\partial Z - \partial \widetilde{W}/\partial Y$ satisfies $\widetilde{\boldsymbol{V}} \cdot \nabla_T \widetilde{\Omega} = R + \nabla_T^2 \widetilde{\Omega}$, with $R = U\widetilde{\Omega} + (Y\partial/\partial Z - Z\partial/\partial Y)(U^2/4 - \Theta/2)$, obtained by eliminating the pressure from the two components of the vector equation (2.23). This transport equation for $\widetilde{\Omega}$, along with equations (2.22) and (2.24) and the Poisson equations for $\widetilde{\Phi}$ and $\widetilde{\Psi}$, were solved using a pseudo-transient method similar to the one of §2.1. Some temperature and streamwise velocity contours, as well as an arrow vector field representing the (original) Cartesian transverse velocities (W, V), are displayed in figure 4 for $\sigma = 1$. Here the streamwise velocity U acts as a sink for the transverse flow, in agreement with (2.21). Contrary to the case of an inclined wall, an appreciable fraction of the fluid being ingested by the wall plume comes now from the sides and is affected by the presence of the wall, cf. the region of low transverse velocity at the lower right of figure 4.

Some properties of the solution are given in figure 5 as functions of the Prandtl number. The general appearance of this figure is similar to that of figure 3. In the asymptotic limits of small and large Prandtl numbers, the scales of the variables $(|\boldsymbol{X}|, U, |\widetilde{\boldsymbol{V}}|, \Theta, P)$ in the thermal region, obtained from the same balances used in the previous subsection, are $(\sigma^{-3/4}, \sigma^{1/2}, \sigma^{-1/4}, \sigma, \sigma^{-1/2})$ for $\sigma \to 0$ and $(\sigma^{-1/2}, 1, \sigma^{-1/2}, \sigma, 1)$ for $\sigma \to \infty$. This yields $\left(\int_0^\infty \int_{-\infty}^\infty U \,\mathrm{d}Z \,\mathrm{d}Y, \int_0^\infty \int_{-\infty}^\infty U^2 \,\mathrm{d}Z \,\mathrm{d}Y\right)$ of orders $(\sigma^{-1}, \sigma^{-1/2})$ for $\sigma \to 0$ and $(1, \sigma^{-1})$ for $\sigma \to \infty$ (where use has been made of the estimates $|\boldsymbol{X}| = O(\sigma^{1/2})$ and $U = O(\sigma^{-1})$ in the outer isothermal viscous region in the second case), in agreement with the trends shown in figure 5. Notice, in particular, that the proportionality of Θ and σ predicted by the scaling analysis for both large and small values of σ is well displayed by $\Theta(0,0)$ over the whole range of σ in figure 5.

The scales (2.20) do not agree with the experimental results of Carey & Mollendorf (1977) mentioned in the Introduction. This is probably because their measurements could be carried out only at moderate distances downstream of the source, where apparently the flow is intermediate between a two-dimensional plume and

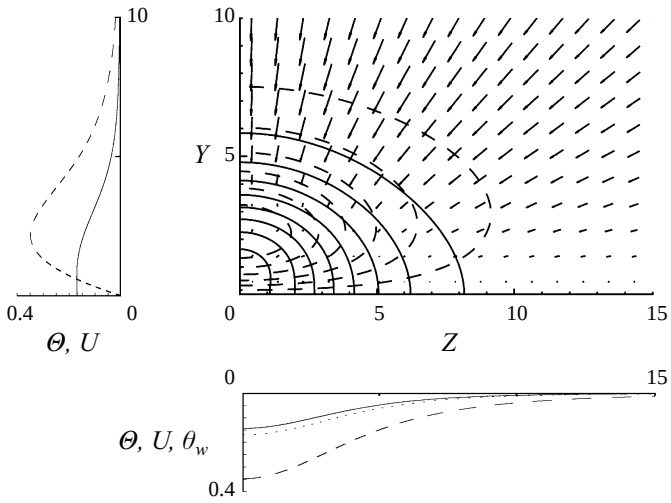

FIGURE 4. Eight equispaced isotherms between $\Theta = 0.02$ and 0.16 (solid) and six equispaced contours of the streamwise velocity between $U = 0.05$ and 0.3 (dashed), for $\sigma = 1$. The arrows represent the transverse velocity field (W, V). Also plotted are temperature (solid) and streamwise velocity (dashed) profiles at the centreplane (left) and on a section parallel to the wall across the maximum of the streamwise velocity (bottom). The dotted curve in this last graph gives the wall temperature profile.

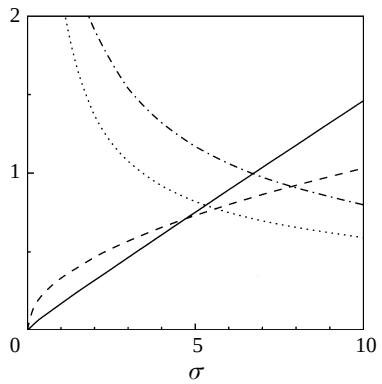

FIGURE 5. Values of $\Theta(0,0)$ (solid), $\partial U/\partial Y(0,0)$ (dashed), $10^{-1} \times \int U \,\mathrm{d}Z \,\mathrm{d}Y$ (dotted), and $\int U^2 \,\mathrm{d}Z \,\mathrm{d}Y$ (dash-and-dot), as functions of the Prandtl number, from the numerical solution of (2.16) and (2.21)–(2.25).

a three-dimensional one. In fact, their results do not seem to provide a consistent description of the far field because the velocity associated with a $\theta \propto x^{-0.77}$ is $u \sim (\theta x)^{1/2} \propto x^{0.115}$, if buoyancy is driving the flow, and then the heat flux increases with x in the form $\phi \propto x^{0.545}$, when in fact ϕ is constant.

The differences between three-dimensional vertical wall plumes and free plumes with regard to their stability characteristics may be less marked than between the nearly two-dimensional flows of §2.1 and two-dimensional free plumes, because the wall does not inhibit the sinuous mode responsible for the strongest instability growth rates of free plumes (Pera & Gebhart 1971; Haaland & Sparrow 1973*a*). Therefore the present flows can be expected to be less stable than the flows of the previous subsection.

2.3. *Isothermal wall*

Assume now that a vertical wall ($\alpha = 0$) is kept at the ambient temperature of the fluid ($\theta = 0$) far from the source. The width of the layer is of the same order as its thickness ($z_c = y_c$ and $w_c = v_c$), as in §2.2, and the balances $u_c/x = w_c/z_c$, $u_c^2/x = \theta_c = \nu u_c/z_c^2$, and $w_c^2 = p_c$, which are based on equations (2.1), (2.2) and (2.3), still apply and relate the scales of all the variables to that of θ. Condition (2.7), however, no longer holds because the heat flux passing a transverse section continuously decreases with increasing x owing to the heat loss at the wall. This leaves the scale of θ undetermined. Assuming an algebraic decay of the form $\theta = \Theta/x^s$, the previous estimates lead to $u = x^{(1-s)/2}U$, $(w, v) = \nu^{1/2}x^{-(1+s)/4}[\widetilde{W} + (1+s)ZU/4, \widetilde{V} + (1+s)YU/4]$ and $p = \nu P/x^{(1+s)/2}$, where the scaled variables depend on $(Z, Y) = (z, y)/(\nu^{1/2}x^{(1+s)/4})$. Substituting all this into the governing equations gives the eigenvalue problem

$$\left.\begin{aligned}
&\nabla_T \cdot \widetilde{\boldsymbol{V}} + U = 0,\\
&\widetilde{\boldsymbol{V}} \cdot \nabla_T U - \frac{s-1}{2}U^2 = \Theta + \nabla_T^2 U,\\
&\widetilde{\boldsymbol{V}} \cdot \nabla_T \widetilde{\boldsymbol{V}} - \frac{3+2s-s^2}{16}U^2\boldsymbol{X} = -\nabla_T P - \frac{1+s}{4}\Theta\boldsymbol{X} + \nabla_T^2\widetilde{\boldsymbol{V}} + \frac{1+s}{2}\nabla_T U,\\
&\widetilde{\boldsymbol{V}} \cdot \nabla_T \Theta - sU\Theta = \frac{1}{\sigma}\nabla_T^2\Theta,\\
&Y = 0:\ U = \widetilde{W} = \widetilde{V} = \Theta = 0,\\
&(|Z|, Y) \to \infty:\ U = \widetilde{W} = \widetilde{V} = \Theta = P = 0,
\end{aligned}\right\} \tag{2.26}$$

to determine s and the scaled variables. This is the defining feature of self-similar solutions of the second kind (see e.g. Barenblatt 1996).

The heat flux (2.7) is now

$$\phi = \nu x^{1-s}\int_0^\infty \int_{-\infty}^\infty U\Theta \,\mathrm{d}Z\,\mathrm{d}Y,$$

and the condition that it decrease with increasing x provides the lower bound $s > 1$ on the eigenvalue s.

An approximation to the eigenvalue s is obtained here in an indirect way. Instead of trying to solve problem (2.26), equations (2.1)–(2.5) with $\alpha = 0$, the Laplacian reduced to $\partial^2/\partial z^2 + \partial^2/\partial y^2$, and $\partial p/\partial x$ suppressed from (2.2), are integrated numerically marching in x with boundary conditions (2.6) except that $\theta = 0$ at $y = 0$, using as initial conditions the solution of (2.16) and (2.21)–(2.25) obtained in §2.2. The numerical treatment of this problem is analogous to that of the previous subsection in that the same decomposition of the transverse velocity is used to eliminate the pressure. The place of $\partial u/\partial t$, which would be added to the left-hand side of (2.2) for the pseudo-transient method, is taken now by $u\partial u/\partial x$, and similarly for the other equations. The solution thus obtained describes the flow on a wall that is adiabatic up to a certain distance from the source and is kept at ambient temperature farther downstream. This solution shows that $\max_{z,y}\theta$, $\max_{z,y} u$, and ϕ all decay as powers of x for sufficiently large values of this variable, and s is obtained by fitting the power laws x^{-s}, $x^{(1-s)/2}$ and x^{1-s}, respectively, to the decaying quantities. The resulting $s(\sigma)$ is given in figure 6.

The two-dimensional analogue of (2.26), describing the flow far downstream of a two-dimensional source, is also of interest. This problem is found by setting $\widetilde{W} +$

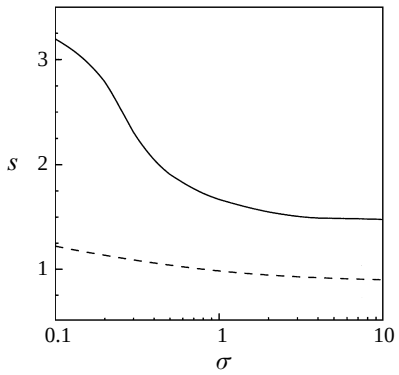

FIGURE 6. Eigenvalues of problem (2.26) (solid) and (2.27) (dashed) as functions of the Prandtl number.

$(1+s)ZU/4 = \partial/\partial Z = 0$ in (2.26) and can be conveniently rewritten in terms of the scaled stream function $F = \psi/(\nu^{1/2}x^{(3-s)/4})$, so that $U = F_Y$, $\widetilde{V} = -(3-s)F/4$, and

$$\left.\begin{aligned} &F_{YYY} + \frac{3-s}{4}FF_{YY} + \frac{s-1}{2}F_Y^2 + \Theta = 0, \\ &\frac{1}{\sigma}\Theta_{YY} + \frac{3-s}{4}F\Theta_Y + sF_Y\Theta = 0, \\ &Y = 0: \ F = F_Y = \Theta = 0; \quad Y \to \infty: \ F_Y = \Theta = 0. \end{aligned}\right\} \tag{2.27}$$

Problem (2.27) was solved using a Newton method and the resulting $s(\sigma)$ is included in figure 6. The condition that the heat flux decrease with x implies only that $s > 3/5$ for a line source, and values $s < 1$ are obtained for σ greater than about 0.76. According to the current scaling this corresponds to streamwise velocities increasing with x, which can never happen for a point source. Thus two-dimensional air flows ($\sigma \approx 0.72$) have $\partial u/\partial x < 0$ but small whilst water flows ($\sigma \approx 7$) have $\partial u/\partial x > 0$.

That the eigenvalues of (2.26) for a point source are found to be uniformly larger than those of (2.27) for a line source was to be expected for the same reason that the temperature on an adiabatic wall decreases more rapidly in the former case than in the latter ($1/x$ versus $1/x^{3/5}$): the spanwise spreading of the three-dimensional flow distributes the heat flux ϕ, or what remains of it, over a larger mass flux than in the two-dimensional flow.

A self-similar solution of the second kind should also exist for a point source on an inclined downward-facing isothermal ambient-temperature wall. The corresponding eigenvalue problem can be easily set up using the order of magnitude estimates of §2.1 that were based on equations (2.1)–(2.5), along with the assumption $\theta \sim x^{-s}$. However, the pseudo-transient technique used in the remainder of this paper proved inadequate to solve the boundary layer problem, because its solution, if it exists, would include a region of unstably stratified fluid adjacent to the wall, and the long-wavelength part of its instability is captured by the boundary layer approximation. This negative result suggests that in many cases in which there is a component of gravity normal to the isothermal wall the asymptotic self-similar solution may not be attained before instability sets in. Likewise, the flow due to a line source of heat on an isothermal downward-facing wall, whose asymptotic self-similar form is given by problem (2.27) as for a vertical wall, and has a Grashof number proportional to

$x^{(3-s)/2}$, should be expected to develop a vortex instability in the region of unstable stratification (Sparrow & Husar 1969; Lloyd & Sparrow 1970).

3. Darcian flows

3.1. *Adiabatic wall*

Consider now the problem of an isolated heat source on an inclined, downward-facing wall of infinite extent in an unbounded fluid-saturated porous medium of permeability K and thermal diffusivity κ. Using the same notation as in the problems discussed previously, the equations describing the flow far downstream of the heat source are

$$\nabla \cdot \boldsymbol{u} = 0, \tag{3.1}$$

$$\frac{\nu}{K} u = -\frac{\partial p}{\partial x} + \theta \cos\alpha, \tag{3.2}$$

$$\frac{\nu}{K} w = -\frac{\partial p}{\partial z}, \tag{3.3}$$

$$\frac{\nu}{K} v = -\frac{\partial p}{\partial y} - \theta \sin\alpha, \tag{3.4}$$

$$\boldsymbol{u} \cdot \nabla \theta = \kappa \nabla^2 \theta, \tag{3.5}$$

to be solved with the boundary conditions

$$\left.\begin{aligned} &y = 0 : \ v = \frac{\partial \theta}{\partial y} = 0, \\ &(|z|, y) \to \infty : \ \boldsymbol{u} = \boldsymbol{0}, \quad \theta = p = 0, \end{aligned}\right\} \tag{3.6}$$

and the integral constraint for the heat flux

$$\int_{-\infty}^{\infty} \int_{0}^{\infty} u\theta \, \mathrm{d}z \, \mathrm{d}y = \phi. \tag{3.7}$$

The scales $[z_c, y_c, u_c, w_c, \theta_c, p_c]$ are obtained from the following order of magnitude estimates: the continuity equation (3.1) gives $u_c/x = w_c/z_c$; balancing u with the driving buoyancy force in (3.2) yields $u_c = K\theta_c \cos\alpha/\nu$; balancing the pressure gradient with buoyancy in (3.4) furnishes the characteristic pressure $p_c = y_c\theta_c \sin\alpha$; invoking this result in (3.3) gives $w_c = Ky_c\theta_c \sin\alpha/\nu z_c$; a balance of advection with plate-normal diffusion in the energy equation (3.5) requires $u_c/x = \kappa/y_c^2$; closure of the system is obtained from (3.7) which yields $u_c\theta_c z_c y_c = \phi$. Solution of these equations gives

$$\left.\begin{aligned} z_c &= \frac{x \tan\alpha}{Q^{1/5}}, \quad y_c = \frac{x \tan\alpha}{Q^{2/5}}, \\ u_c &= \frac{Q^{4/5}\kappa}{x(\tan\alpha)^2}, \quad w_c = \frac{Q^{3/5}\kappa}{x \tan\alpha}, \\ \theta_c &= \frac{\phi}{Q^{1/5}\kappa x}, \quad p_c = \frac{\kappa\nu Q^{2/5}}{K}, \end{aligned}\right\} \tag{3.8}$$

where now $Q = Ra \sin\alpha \tan\alpha$ and $Ra = \phi K/\nu\kappa^2$ is a Rayleigh number. As can be seen, $y_c \ll z_c \ll x$ for $Ra \gg 1$ and $\alpha \gg Ra^{-1/2}$. In this event the pancake-like structure

shown in figure 1 exists, irrespective of the fact that both transverse boundary layer coordinates scale linearly with x. Transforming variables according to (2.9) and then defining $\widetilde{W} = W - ZU$ and $\widetilde{V} = V - YU$ furnishes the problem governing the transverse structure of the flow:

$$\nabla_T \cdot \widetilde{V} + U = 0, \tag{3.9}$$

$$U = \Theta, \tag{3.10}$$

$$\widetilde{W} = -\frac{\partial P}{\partial Z} - ZU, \tag{3.11}$$

$$\frac{\partial P}{\partial Y} = -\Theta, \tag{3.12}$$

$$\widetilde{V} \cdot \nabla_T \Theta - U\Theta = \frac{\partial^2 \Theta}{\partial Y^2}, \tag{3.13}$$

$$Y = 0: \ \widetilde{V} = \frac{\partial \Theta}{\partial Y} = 0; \quad (|Z|, Y) \to \infty: \ U = \widetilde{W} = \Theta = P = 0, \tag{3.14}$$

$$\int_0^\infty \int_{-\infty}^\infty U\Theta \, \mathrm{d}Z \, \mathrm{d}Y = 1. \tag{3.15}$$

From the numerical solution of this parameter-free problem, $\Theta_{max} \approx 0.667$ (attained at $Z = Y = 0$) and $\int_0^\infty \int_{-\infty}^\infty U \, \mathrm{d}Z \, \mathrm{d}Y \approx 3.996$.

As for Newtonian flow, the problem with $\alpha < 0$ has no solution and the fluid separates from the wall forming a free buoyant plume. When $\alpha = 0$ the flow is not affected by the presence of the wall and the solution coincides with (half of) the classical solution of Wooding (1963) for an axisymmetric plume.

3.2. *Isothermal wall*

Condition (3.7) is not applicable when the wall is held at ambient temperature far downstream of the source, and then the scales of the variables in the asymptotic self-similar solution cannot be determined *a priori*. In addition, the temperature of the fluid increases with y in a region adjacent to the wall, rendering this solution unstable when $\alpha > 0$. If $\alpha = 0$ (vertical wall) the assumption $\theta = (\nu/K)U/x^s$, with s to be determined, and the order of magnitude balances of terms in conservation equations (3.1)–(3.5) yield $u = U/x^s$, $(w, v) = \kappa^{1/2} x^{-(1+s)/2}[\widetilde{W} + (1+s)ZU/2, \widetilde{V} + (1+s)YU/2]$, $p = (\kappa\nu/K)P$, and $(z, y) = \kappa^{1/2} x^{(1+s)/2}(Z, Y)$. The eigenvalue s and the scaled variables are then determined by the condition that the problem

$$\left.\begin{aligned} &\nabla_T \cdot \widetilde{V} + U = 0, \\ &\widetilde{V} = -\nabla_T P - \frac{1+s}{2} U\boldsymbol{X}, \\ &\widetilde{V} \cdot \nabla_T U - sU^2 = \nabla_T^2 U, \\ &Y = 0: \ U = \widetilde{V} = 0, \\ &(|Z|, Y) \to \infty: \ U = \widetilde{W} = \widetilde{V} = P = 0, \end{aligned}\right\} \tag{3.16}$$

have a non-trivial solution. Each eigensolution corresponds to a heat flux passing a transverse section proportional to x^{1-s}, and the condition that the heat flux decrease with x (on account of the heat lost to the wall) implies $s > 1$. This, in turn, justifies the boundary layer approximation made neglecting $\partial p/\partial x$ in (3.2) to obtain (3.16). An approximate numerical solution of (3.16), obtained as for the Newtonian flow, yields $s \approx 1.8$.

The analogous problem for a two-dimensional source, obtained by setting $\widetilde{W} = -(1+s)Z\,U/2$ and suppressing the Z-derivatives of U and P from (3.16), reduces to

$$\left.\begin{array}{ll} \widetilde{V}_{Y} + \dfrac{1-s}{2}U = 0, & (\widetilde{V}U)_{Y} + \dfrac{1-3s}{2}U^2 = U_{YY}, \\ Y = 0: \ U = \widetilde{V} = 0; & Y \to \infty: \ U = 0. \end{array}\right\} \tag{3.17}$$

Owing to the proportionality of θ and u, problem (3.17) coincides with the one describing the self-similar flow in a two-dimensional wall jet (Glauert 1956), for which $s = 1/2$. This result can be retrieved by integrating the second equation (3.17) over the range (Y, ∞), multiplying by U, using the first equation (3.17) to eliminate $\widetilde{V}$, and integrating again over the entire boundary layer to obtain $(1-2s)\int_0^\infty U\left(\int_{Y_1}^\infty U^2\,\mathrm{d}Y_2\right)\mathrm{d}Y_1 = 0$.

The work of F.J.H. was partially supported by the DGICYT under grants PB95-0008 and PB94-0400. P.D.W. acknowledges support from the Spanish Ministry of Education and Culture for a three month visit to ETS Ingenieros Aeronáuticos in Madrid, under contract SAB95-0514.

REFERENCES

Aung, W. 1988 *Cooling Technology for Electronic Equipment*. Hemisphere.

Azfal, N. 1980 Convective wall plume: Higher order analysis. *Intl J. Heat Mass Transfer* **23**, 505–513.

Barenblatt, G. I. 1996 *Scaling, Self-similarity, and Intermediate Asymptotics*. Cambridge University Press.

Bickley, W. G. 1937 The plane jet. *Phil. Mag.* (7) **23**, 727–731.

Buckmaster, J. 1973 Viscous-gravity spreading of an oil slick. *J. Fluid Mech.* **59**, 481–491.

Carey, V. P. & Mollendorf, J. C. 1977 The temperature field above a concentrated heat source on a vertical adiabatic surface. *Intl J. Heat Mass Transfer* **20**, 1059–1067.

Chen, T. S. & Tzuoo, K. L. 1982 Vortex instability of free convection flow over horizontal and inclined surfaces. *Trans. ASME J. Heat Transfer* **104**, 637–643.

Daniels, P. G. 1992 A singularity in thermal boundary-layer flow on a horizontal surface. *J. Fluid Mech.* **242**, 419–440.

Dring, R. P. & Gebhart, B. 1968 A theoretical investigation of disturbance amplification in external laminar natural convection. *J. Fluid Mech.* **34**, 551–564.

Gebhart, B., Jaluria, Y., Mahajan, R. L. & Sammakia, B. 1988 *Buoyancy-Induced Flows and Transport*. Hemisphere.

Glauert, M. B. 1956 The wall jet. *J. Fluid Mech.* **1**, 625–643.

Haaland, S. E. & Sparrow, E. M. 1973*a* Stability of buoyant boundary layers and plumes, taking account of nonparallelism of the basic flows. *Trans. ASME J. Heat Transfer* **95**, 295–301.

Haaland, S. E. & Sparrow, E. M. 1973*b* Wave instability of natural convection on inclined surfaces accounting for nonparallelism of the basic flow. *Trans. ASME J. Heat Transfer* **95**, 405–407.

Higuera, F. J. 1993 Natural convection flow below a downward facing horizontal plate. *Eur. J Mech.* B **12**, 289–311.

Jaluria, Y. & Gebhart, B. 1977 Buoyancy-induced flows arising from a line thermal source on an adiabatic vertical surface. *Intl J. Heat Mass Transfer* **20**, 153–157.

KAKAC, S., YÜNCÜ, H. & HIJIKATA, K. 1994 *Cooling of Electronic Systems*. NATO ASI Series E, vol. 258. Kluwer.

KIM, S. J. & LEE, S. W. 1996 *Air Cooling Technology for Electronic Equipment*. CRC Press.

LIBURDY, J. A. & FAETH, G. M. 1975 Theory of a steady laminar thermal plume along a vertical adiabatic wall. *Lett. Heat Mass Transfer* **2**, 407–418.

LISTER, J. R. 1992 Viscous flows down an inclined plane from point and line sources. *J. Fluid Mech.* **242**, 631–653.

LLOYD, J. R. & SPARROW, E. M. 1970 On the instability of natural convection flow on inclined plates. *J. Fluid Mech.* **42**, 465–470.

NACHTSHEIM, P. R. 1963 Stability of free convection boundary layer flows. *NASA TN* D-2089.

NIELD, D. A. & BEJAN, A. 1992 *Convection in Porous Media*. Springer.

PERA, L. & GEBHART, G. 1971 On the stability of laminar plumes: some numerical solutions and experiments. *Intl J. Heat Mass Transfer* **14**, 975–984.

SCHLICHTING, H. 1960 *Boundary Layer Theory*. McGraw-Hill.

SPARROW, E. M. & HUSAR, R. B. 1969 Longitudinal vortices in natural convection flow on inclined plates. *J. Fluid Mech.* **37**, 251–255.

SPARROW, E. M., PATANKAR, S. V. & ABDUL-WAHED, R. M. 1978 Development of wall and free plumes above a heated vertical plate. *Trans. ASME J. Heat Transfer* **100**, 184–190.

WOODING, R. A. 1963 Convection in a saturated porous medium at large Rayleigh number or Peclet number. *J. Fluid Mech.* **15**, 527–544.

ZELDOVICH, YA. B. 1937 The asymptotic laws of freely-ascending convective flows. *Z. Eksperimental-noi Teoreticheskoi Fiziki* **7**, 1463–1465. (See also *Selected Works of Yakov Borisovich Zeldovich*, Princeton University Press, 1992.)

ZIMIN, V. D. & LYAKHOV, YU. N. 1970 Convective wall plume. *J. Appl. Mech. Tech. Phys.* **11**, 511–513.